GEOPHYSICAL RESEARCH, 2018, vol. 19, no. 3, pp.57-72. https://doi.org/10.21455/gr2018.3-4

UDC 539.3, 539.4.01

ESTIMATION OF ROCK STRENGTH PROPERTIES FROM TRIAXIAL TEST DATA

I.A. Garagash[1], N.V. Dubinya[1], O.A. Rusina[1,2], S.A. Tikhotsky[1], I.V. Fokin[1]

[1] *Schmidt Institute of Physics of the Earth, the Russian Academy of Sciences, Moscow, Russia*
[2] *Lomonosov Moscow State University, Moscow, Russia*

Abstract. The article is devoted to usage of non-associated plastic flow law for describing deformation processes occurring in rock masses subjected to external stresses. The constitutive relations are formulated for a rock mass being subjected to stresses exceeding its elasticity limit. The concept of friction angle being a function of accumulated plastic strain is used to describe deformation process. The experimentally obtained stress-strain curves provided by series of triaxial tests carried out for fractured rock samples are considered within the formulated model. It is shown that usage of non-associated plastic flow law gives an opportunity to describe the experimental results more precisely compared to standard methods such as Mohr–Coulomb model. Numerical simulation presented in the article provides an image of plastic deformation localization taking place in rocks in natural conditions. The physical mechanism of plastic deformation accumulation through emergence of fractures and reactivation and propagation of pre-existing fractures is proposed. The fracture system evolution model tendency is revealed for conditions of triaxial test: it is shown that propagating fractures are to be specifically spatially oriented as the angle between normal vectors to them and the symmetry axis can be calculated. As far as the concept of changing friction angle is used, the spatial orientations and relative number of propagating fractures in rock masses can be qualitatively and quantitatively determined at each moment of deformation process. The proposed model of fractured rocks' deformation under applied external stresses is tested using experimental data and can be used for a more precise description of rheology while dealing with geomechanical problems.

Keywords: geomechanical modeling, strength properties of rocks, non-associated law of plastic flow, variable angle of internal friction.

Introduction

Currently, geomechanical modeling has become an important and integral part of developing oil and gas deposits. Geomechanical modelling is impossible without indicating parameters of the medium – elastic properties, rock strength, angle of internal friction [*Garagash et al*., 2015]. Knowledge of mechanical properties makes possible to calculate the stress and deformation distributions and carry out their complex interpretation with geological and geophysical data.

Rocks that form the sedimentary mass have different mechanical properties. This causes a nonuniform distribution of stresses and appearance of areas of their anomalous values exceeding rock strength. In such conditions drilling of wells is accompanied by rock destruction.

An adequate model of rock behavior is a non-associated law of plastic flow with Mohr-Coulomb or Drucker-Prager flow condition. In order to correctly describe the specific collector, a number of triaxial tests should be performed to determine the dependence of medium parameters (shear modulus, Poisson's ratio, cohesion and friction) on stress-state parameters (load and plastic deformation). Such approach was used to determine the mechanical properties of sandrock with increased porosity [*Garagash, Nikolaevski, Dudley*, 1999].

Model of non-associated plastic flow

Plastic deformation of rocks is caused to intergranular sliding and microcracking. Since implementation of such deformations needs friction to be overcame, plastic flow significantly

depends on the level of average stresses $\sigma = \frac{1}{3}\sigma_{ii} = \frac{1}{3}(\sigma_1 + \sigma_2 + \sigma_3)$, and for its description the Mohr-Coulomb or Drucker-Prager conditions are often used, written as follows:

$$T + \alpha\sigma = c, \tag{1}$$

where $T = (s_{ij}s_{ij})^{1/2}$ is shear stress intensity ($s_{ij} = \sigma_{ij} - \delta_{ij}\sigma$ are components of deviatoric stresses); $\alpha = \sin\varphi$ is friction coefficient (φ is angle of internal friction); c is cohesion.

Let's proceed from the fact that tensor components of deformation increments $d\varepsilon_{kl}$ and tensor components of stress increments $d\sigma_{ij}$ are related by equations [*Nikolaevskii*, 1971]

$$d\varepsilon_{ij} = \Pi_{ijkl} d\sigma_{kl}, \tag{2}$$

where

$$\Pi_{ijkl} = \left[-\frac{\nu}{2G(1+\nu)}\delta_{ij}\delta_{kl} + \frac{1}{4G}\left(\delta_{ik}\delta_{jl} + \delta_{kj}\delta_{il}\right)\right] + \frac{1}{4H}\left(N_{ij} + \frac{2}{3}\Lambda\delta_{ij}\right)\left(N_{kl} + \frac{2}{3}\alpha\delta_{kl}\right); \tag{3}$$

in (3) ν is Poisson's ration; G is shear modulus; H is modulus of plastic hardening; $N_{ij} = \frac{s_{ij}}{T}$.

Parameter Λ from (3) is called a coefficient of dilatancy and characterizes inelastic change of volume caused by shear deformation. To take dilatancy effect into account the following ratio was introduced:

$$d\varepsilon^{pl} = \Lambda d\Gamma^{pl}, \tag{4}$$

where $d\Gamma^{pl}$ is plastic shear strain increments intensity; $d\Gamma^{pl} = 2\left[\left(d\varepsilon_{ij}^{pl} - \frac{1}{3}\delta_{ij}d\varepsilon^{pl}\right)\left(d\varepsilon_{ij}^{pl} - \frac{1}{3}\delta_{ij}d\varepsilon^{pl}\right)\right]^{1/2}$ [*Nikolaevskii*, 1971].

Reversing the relation (3), we obtain another representation of constitutive law [*Rudnicki*, *Rice*, 1975]:

$$\Delta\sigma_{ij} = E_{ijkl}\Delta\varepsilon_{kl}, \tag{5}$$

$$E_{ijkl} = G\left\{\left[\left(\delta_{ik}\delta_{jl} + \delta_{il}\delta_{jk}\right) + \left(\frac{K}{G} - \frac{2}{3}\right)\delta_{ij}\delta_{kl}\right] - \right.$$
$$\left. - \frac{G}{(H+G) + \alpha\Lambda K}\left(N_{ij} + \frac{K}{G}\Lambda\delta_{ij}\right)\left(N_{kl} + \frac{K}{G}\Lambda\delta_{kl}\right)\right\}, \tag{6}$$

where $K = \frac{2(1+\nu)}{3(1-2\nu)}G$ is bulk compression modulus.

Given representations of the constitutive law (2) and (5) generalize the Prandtl – Reuss equations in case of medium with internal friction and dilatancy.

Plastic hardening modulus H from (2) and (5) connects increments of average stresses $d\sigma$ and shear stress intensity dT with plastic shear strain increments intensity

$$d\Gamma^{pl} = \frac{1}{H}(dT + \alpha d\sigma). \tag{7}$$

Typical diagram of rock deformation shows shear stress intensity changes T with an increase in total intensity of deformations Γ (Fig. 1, *left)*. Inelastic deformation occurs after reaching the elasticity limit T_{pl} and is accompanied by the development of pre-existing cracks and formation of new ones. At the same time effective mechanical properties gradually de-

crease and material softening occurs, manifested in implementation of descending branch of deformation diagram.

If we rearrange the deformation diagram in $T-\Gamma^{pl}$ axes, it will take the form shown in Fig. 1, *right.* In this case plastic hardening modulus H is equal to tangent of the curve slope.

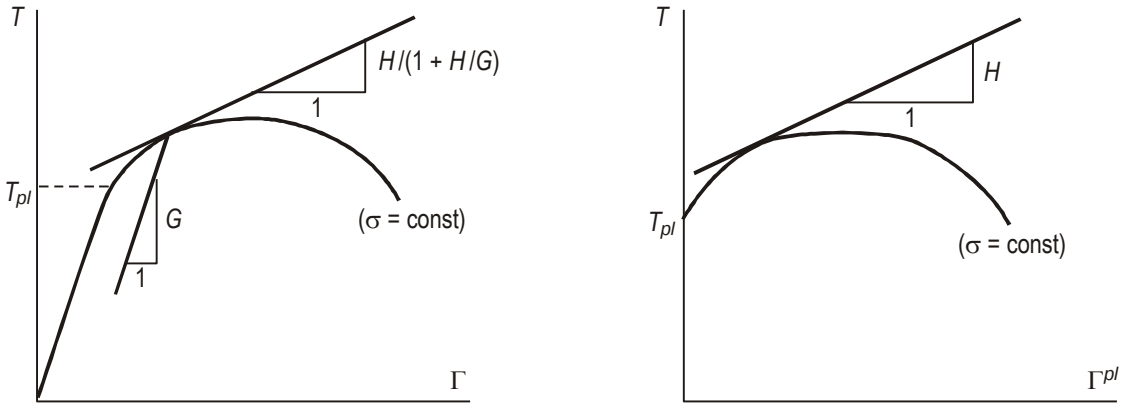

Fig. 1. Deformation diagram in $T-\Gamma$ axes (*left*) and $T-\Gamma^{pl}$ axes (*right*)

According to triaxial tests [*Rice*, 1979], for rocks parameter α usually has a value of 0.4–0.9 and parameter Λ – 0.2–0.4.

There are noticeable changes in the distribution of fractures after the peak stress is reached – fractures of preferred orientation emerge caused by partial closure of some fractures and rapid growth of the others, and also a phenomenon that is called a plastic deformation localization takes place [*Garagash, Nikolaevskii*, 1989; *Garagash*, 2006].

In Fig. 1, *right* it can be seen that modulus of plastic hardening H is not a constant and changes with accumulation of inelastic deformation [*Vermeer, de Borst*, 1984]. Indeed, if we integrate the ratio (7), we will obtain the plastic condition of Drucker-Prager in the form

$$T+\alpha\sigma=f\,, \tag{8}$$

where f is yield function defined by the expression

$$f=\int\limits_{\Gamma^{pl}} H d\Gamma^{pl}+\int\limits_{\alpha}\sigma d\alpha+c\,, \tag{9}$$

where c is cohesion.

If it is postulated that f=const for the problem, it will be clear from (9) that friction angle is to constant, modulus of plastic hardening is to be equal to 0. It means that the friction coefficient change during deformation and modulus of plastic hardening H is a function of α. We will proceed from the fact that parameter α depends not only on the average stress, but also on the accumulated plastic deformation, i.e. $\alpha=\alpha(\Gamma^{pl},\sigma)$. In this case

$$d\alpha=\frac{\partial\alpha}{\partial\Gamma^{pl}}d\Gamma^{pl}+\frac{\partial\alpha}{\partial\sigma}d\sigma\ , \tag{10}$$

and expression for the stream function (8) can be rewritten as

$$f=\int\limits_{\Gamma^{pl}}(H+\sigma\frac{\partial\alpha}{\partial\Gamma^{pl}})d\Gamma^{pl}+\int\limits_{\sigma}\sigma\frac{\partial\alpha}{\partial\sigma}d\sigma+c\,. \tag{11}$$

If we assume that

$$f=c+\int\limits_{\sigma}\sigma\frac{\partial\alpha}{\partial\sigma}d\sigma\,, \tag{12}$$

then for the modulus of plastic hardening we obtain the expression [Garagash, 2006]

$$H = -\sigma \frac{d\alpha}{d\Gamma^{pl}} \quad . \tag{13}$$

Since, according to (13), H varies in proportion to the average stress, then its value will depend on the transition path from one point of the stress space to another.

Laboratory studies of mechanical properties of rocks

Triaxial compression tests, described in detail in [Tikhotsky et al., 2017], were carried out on servohydraulic test unit *GCTS RTR*4500. This work discusses the results obtained for four cylindrical samples with diameter of 30 mm and length of 60 mm that were made (cut) from the core. Samples were placed in thermocontractable jacket with induction sensors that measure axial and radial changes in linear dimensions, and then were put in stabilometer filled with hydraulic oil, which pressure ensured uniform compression of the sample; along the vertical axis it was loaded by an axial manipulator of installation (Fig. 2).

Maximum principal stress σ_1, standing for the sum of hydraulic oil pressure and pressure generated by the axial manipulator, acts along the vertical axis of the sample. Radial stress $\sigma_r = \sigma_2 = \sigma_3$, which is the hydraulic oil pressure, acts on the lateral surface of the sample.

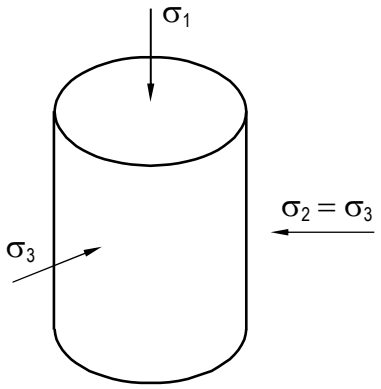

Fig. 2. Loading scheme in three-axial test. σ_1 – maximum principal stress; $\sigma_2=\sigma_3$ – radial stress σ_r (caused by hydraulic oil pressure)

Tests on rock samples were carried out according to the multistage loading scheme [*Kim, Ko,* 1979]. First of all, hydraulic oil pressure rose to the first preset value; the sample was maintained at this constant pressure until its linear dimensions stabilized. Then, the sample was compressed by the axial manipulator so that deformation rate was constant and equal to 10^{-5} 1/s.

Loading was stopped when the limit of linear elasticity was reached, after that the sample was unloaded. Further, oil pressure was increased until the next preset value – loading-unloading cycle was repeated. On the last cycle the sample was transferred beyond the strength limit.

Typical experimental deformation diagram of sample 1 is given in Fig. 3.

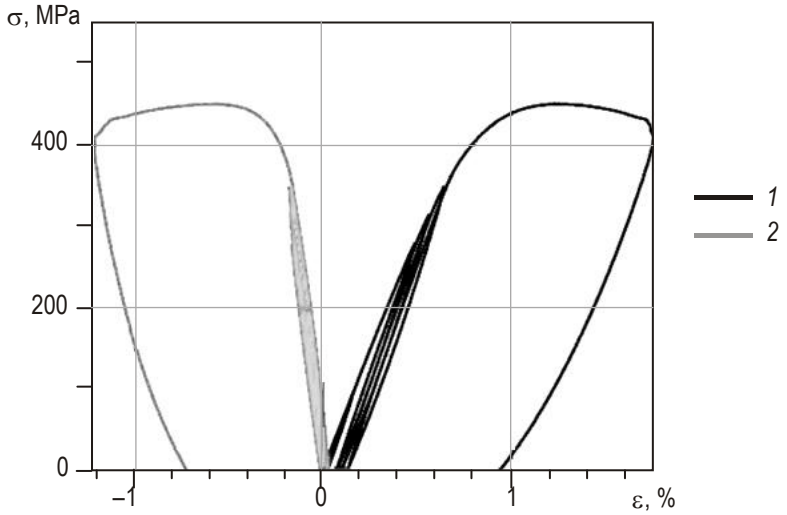

Fig. 3. Experimental deformation curve for three-axial test 1. Differential axial stress (*1*) and radial stress (*2*)

The following parameters were measured during the test: radial strain ($\varepsilon_r = \varepsilon_{22} = \varepsilon_{33}$), axial strain ($\varepsilon_a = \varepsilon_{11}$), axial stress ($\sigma_a = \sigma_{11} = \sigma_1$), radial stress ($\sigma_r = \sigma_{22} = \sigma_{33} = \sigma_2 = \sigma_3$), volume deformation ($\theta = \varepsilon_{ii} = \varepsilon_{11} + \varepsilon_{22} + \varepsilon_{33}$). The obtained dependences of stresses on strain allow to draw conclusions about the rheology of test rock sample under conditions simulating formations.

Referring to Fig. 3, we will describe the method for determining mechanical properties of rocks using the results of triaxial tests conducted on sample 1. As it was shown above the axial stress σ_{11} increases with equal lateral stresses $\sigma_{22} = \sigma_{33}$ in the test sample (see Fig. 2). Behavior of the sample within the limits of elasticity is determined by Hooke's law:

$$\varepsilon_{11} = \frac{1}{E}(\sigma_{11} - 2\nu\sigma_{33}),\ \ \varepsilon_{22} = \varepsilon_{33} = \frac{1}{E}\left[\sigma_{33} - \nu(\sigma_{11} + \sigma_{33})\right], \tag{14}$$

where E is Young's modulus.

To determine shear modulus $G = \dfrac{E}{2(1+\nu)}$ and Poisson's ratio ν it is necessary to proceed as follows. Let's consider the deformation increments on the elastic part of deformation curve. Stress increments are denoted by $\Delta\sigma_{ij}$ and elastic deformation increments are denoted by $\Delta\varepsilon_{ij}$, so equations (14) take the form

$$\Delta\varepsilon_{11} = \frac{1}{E}(\Delta\sigma_{11} - 2\nu\Delta\sigma_{33}),\ \ \Delta\varepsilon_{22} = \Delta\varepsilon_{33} = \frac{1}{E}\left[\Delta\sigma_{33} - \nu(\Delta\sigma_{11} + \Delta\sigma_{33})\right]. \tag{15}$$

Equations (15) are rewritten as

$$\Delta\varepsilon_{11} = \alpha_1\Delta\sigma_{11} - \alpha_2\Delta\sigma,\ \ \Delta\varepsilon_{33} = \alpha_1\Delta\sigma_{33} - \alpha_2\Delta\sigma, \tag{16}$$

where $\Delta\sigma = \dfrac{1}{3}(\Delta\sigma_{11} + 2\Delta\sigma_{33})$ is an increment of mean stress; $\alpha_1 = \dfrac{1}{2G}$, $\alpha_2 = \dfrac{\nu}{2G(1+\nu)}$.

Solving equations (16), we can find the values

$$\alpha_1 = \frac{\Delta\varepsilon_{11} - \Delta\varepsilon_{33}}{\Delta\sigma_{11} - \Delta\sigma_{33}},\ \ \alpha_2 = \frac{1}{2\Delta\sigma}[\alpha_1(\Delta\sigma_{11} + \Delta\sigma_{33}) - (\Delta\varepsilon_{11} + \Delta\varepsilon_{33})], \tag{17}$$

after that we obtain

$$G = \frac{1}{2\alpha_1}, \quad \nu = \frac{\alpha_2}{\alpha_1 - \alpha_2}. \tag{18}$$

Using relations (17) and (18) given that $\Delta\sigma_{33} = 0$, the expression for G is rewritten as

$$G = \frac{1}{2}\frac{\Delta\sigma_{11}}{\Delta\varepsilon_{11} - \Delta\varepsilon_{33}}, \tag{19}$$

which allows to calculate the shear modulus from experimental data.

Further, with shear modulus obtained, we can find the value of the Young's modulus in accordance with the first equation in (16):

$$E = \frac{\Delta\sigma_{11}}{\Delta\varepsilon_{11}}. \tag{20}$$

Expressions (19) and (20) allow us to determine the Poisson's ratio

$$\nu = \frac{1}{2}\frac{E}{G} - 1. \tag{21}$$

Inelastic deformation of the sample occurs when the Mohr-Coulomb strength criterion for shear stresses is satisfied

$$f^s = 0, \quad f^s = \sigma_1 - \sigma_3 N_\varphi + 2c\sqrt{N_\varphi}, \tag{22}$$

where

$$N_\varphi = \frac{1 + \sin\varphi}{1 - \sin\varphi}. \tag{23}$$

Here σ_3 and σ_1 are maximum and minimum principal stresses ($\sigma_1 < \sigma_2 < \sigma_3$; compressive stresses hereinafter are assumed to be negative).

According to (23), internal friction angle (*IFA*) is defined as

$$\varphi = \arcsin\frac{N_\varphi - 1}{N_\varphi + 1}. \tag{24}$$

Using relations (22), we find

$$N_\varphi = \frac{\sigma_1\sigma_3 + 2c^2}{\sigma_3^2} - \sqrt{\left(\frac{\sigma_1\sigma_3 + 2c^2}{\sigma_3^2}\right)^2 - \frac{\sigma_1^2}{\sigma_3^2}}. \tag{25}$$

For the experimental conditions $\sigma_1 = \sigma_{11}$ and $\sigma_3 = \sigma_{33}$.

Inelastic deformation begins when the elastic limit σ_{11}^{pl} is reached. Assuming that at this moment the cohesion c is overcome at zero friction angle φ, we define the cohesion –

$$c = \frac{1}{2}(\sigma_{33} - \sigma_{11}^{pl}). \tag{26}$$

Further, moving along the deformation curve, according to (25), we calculate parameter N_φ for the selected points using the formula

$$N_\varphi = \frac{\sigma_{11}\sigma_{33} + 2c^2}{\sigma_{33}^2} - \sqrt{\left(\frac{\sigma_{11}\sigma_{33} + 2c^2}{\sigma_{33}^2}\right)^2 - \frac{\sigma_{11}^2}{\sigma_{33}^2}}. \tag{27}$$

Then the friction angles are determined from equation (24).

Finally, we compare each value of the friction angle with the value

$$\varepsilon_i^{pl} = \frac{1}{2}\Gamma^{pl} = \frac{1}{\sqrt{3}}(\varepsilon_{11}^{pl} - \varepsilon_{33}^{pl}). \quad (28)$$

Such treatment of experimental data allows to determine the plastic hardening modulus *H* and take plastic flow of rocks into account in a proper way.

Laboratory results

The described method was verified on data obtained from testing cylindrical rock samples drilled from core. Elastic moduli and strength parameters determined in this case by the standard method[1] are given in Table 1. It should be noted that two fixed strength parameters are not enough to describe the hardening and softening of rocks under loading conditions. Hardening and softening parameters must be calibrated for each specific sample. As it was shown above, the internal friction angle change caused by accumulation of plastic shear strain intensity can be used as such physically based parameter.

Table 1. Elastic moduli and strength parameters determined by the standard method

Sample	Elastic moduli		Strength parameters	
	Young's modulus, GPa	Poisson's ratio	*UCS**, MPa	*IFA***, °
1	60.0	0.33	127.6	27
2	51.6	0.27	77.5	32
3	80.8	0.33	181.1	31
4	45.0	0.26	–	–

* – ultimate compressive strength (from ***U**nconfined **C**ompressive **S**trength*); ** – internal friction angle (from ***I**nternal **F**riction **A**ngle*).

The following mechanical parameters were obtained using the described method of processing the experimental deformation curve (see Fig. 3): *G*=21.889 GPa, *E*=58.331 GPa, ν=0.3324, *c*=146.05 MPa. Dependence of the friction angle on the plastic strain accumulated after overcoming the elasticity limit of $\sigma_{11}^{pl} = 3871.1$ MPa, is given in Table 2.

Table 2. Dependence of friction angle on the accumulated plastic strain

Friction angle, φ°	Plastic strain, ε_i^{pl}
0	0
4.587	0.000028
7.584	0.000061
8.582	0.000082
11.356	0.000342
13.297	0.000764
14.655	0.001298

[1] See ASTM D7012-14e1, Standard Test Methods for Compressive Strength and Elastic Moduli of Intact Rock Core Specimens under Varying States of Stress and Temperatures, ASTM International, West Conshohocken, PA, 2014, www.astm.org

15.556	0.001931
16.125	0.002669
16.457	0.003695
16.519	0.004886
16.445	0.005858
16.278	0.006876
16.019	0.007942

The results obtained from experimental deformation curve were verified by numerical modelling of triaxial sample test. Calculations were carried out using the program code *FLAC*^{3D} [Fast ..., 2006], that implements an explicit finite-difference scheme for solving three-dimensional problems of continuum mechanics. Deformation diagrams given in Fig. 4 were constructed using strength parameters determined by the standard (curve *2*) and proposed (curve *3*) method. It can be seen, that variable angle of friction allowed to simulate the deformation curve close to the real one both for hardening and softening modes.

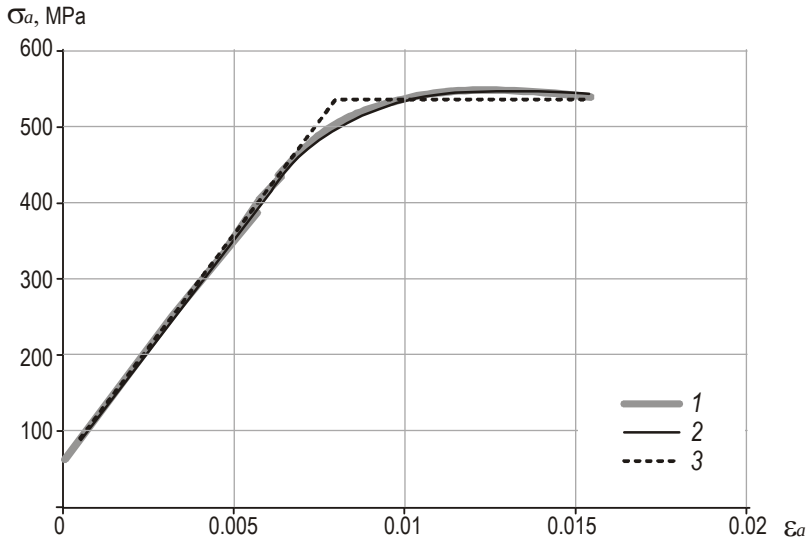

Fig. 4. Experimental (*1*) and model (*2*, *3*) deformation curves. Curve *2* is calculated using parameters, derived by standard ASTM methodic, curve *3* is calculated using approach suggested in this paper

Note that the deformation diagram for the material with strength parameters determined by the standard method (Fig. 4, curve *2*), can be obtained analytically without using numerical solution.

Let's consider the Prandtl-Reuss constitutive equation (5) for material with internal friction and dilatancy which establish a relationship between components of stress increments tensor $d\sigma_{ij}$ and strain increments tensor $d\varepsilon_{kl}$. The stress-strain state of the sample is homogeneous and, therefore, equilibrium equations are satisfied automatically. The constitutive equations are the only thing to consider. In our case $\sigma_{22} = \sigma_{33}$, $\varepsilon_{22} = \varepsilon_{33}$ and $d\sigma_{22} = d\sigma_{33} = 0$. As a result, relationships (5) can be rewritten as

$$\begin{aligned} d\sigma_{11} &= E_{1111} d\varepsilon_{11} + 2E_{1122} d\varepsilon_{22}, \\ 0 &= E_{2211} d\varepsilon_{11} + (E_{2222} + E_{2233}) d\varepsilon_{22}, \end{aligned} \tag{29}$$

where

$$E_{1111} = G\left[\frac{K}{G} - \frac{2}{\sqrt{3}}\frac{K}{G}\alpha\right], \quad E_{2222} + E_{2233} = 2G\left[\frac{K}{G} + \frac{1}{\sqrt{3}}\frac{K}{G}\alpha\right],$$
$$E_{1122} = G\left[\frac{K}{G} - \frac{2}{\sqrt{3}}\frac{K}{G}\alpha\right], \quad E_{2211} = G\left[\frac{K}{G} + \frac{1}{\sqrt{3}}\frac{K}{G}\alpha\right]. \tag{30}$$

Substituting (30) into (29), we obtain $d\sigma_{11} = 0$, and, therefore, after reaching the strength limit, the deformation enters the horizontal "shelf" as it is shown in Fig. 4.

Note, that the usage of the standard constant strength parameters does not allow to display the deformation features observed during the rock loading. Let's show this on the example of compressible elastoplastic stratum, bounded by two elastic layers (Fig. 5). Layers are loaded by vertical pressure; sliding conditions are postulated on the vertical boundaries. Calculation are performed using the program code *FLAC*^{3D} that allows to carry out the calculations for elastoplastic materials with variable strength parameters.

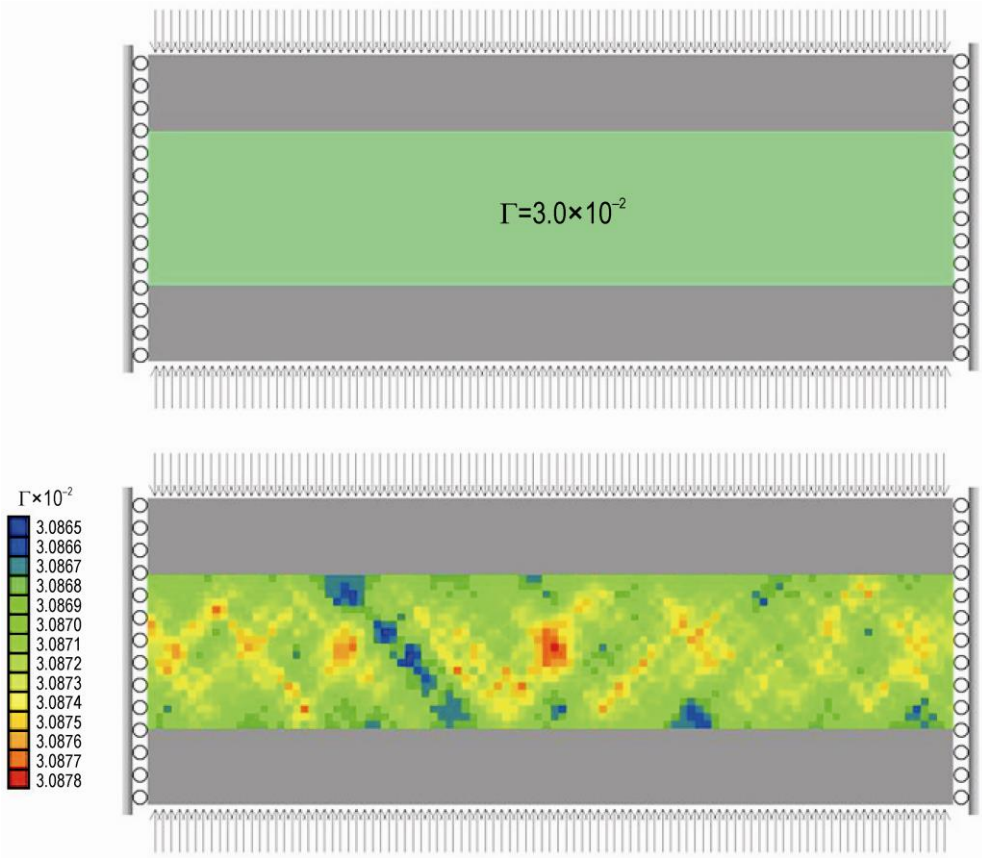

Fig. 5. Calculated amplitude of the shear strain intensity Γ in the elastoplastic layer bounded by two elastic layers (shown in gray). Top: calculated with parameters derived using the standard approach. Bottom: calculated with parameters obtained using the approach presented in the paper. Applied stress direction is shown by arrows at top and bottom. Left – $\Gamma\times10^{-2}$ scale

It can be seen that in the case of using standard constant strength parameters given in Table 1, elastoplastic layer is deformed homogeneously (see Fig. 5, *top*), while in the case of using variable angle of internal friction (see Table 2) deformation beyond the strength limit occurs inhomogeneously and leads to localization of inelastic deformation (see Fig. 5, *bottom*).

The proposed approach to experimental data treatment was verified on a number of samples. The comparison of experimental data (curves *1*) with results of numerical modelling of triaxial tests obtained using the strength parameters determined by the proposed method (curves *2*) for samples 2, 3, 4 (see Table 1) is given in Fig. 6.

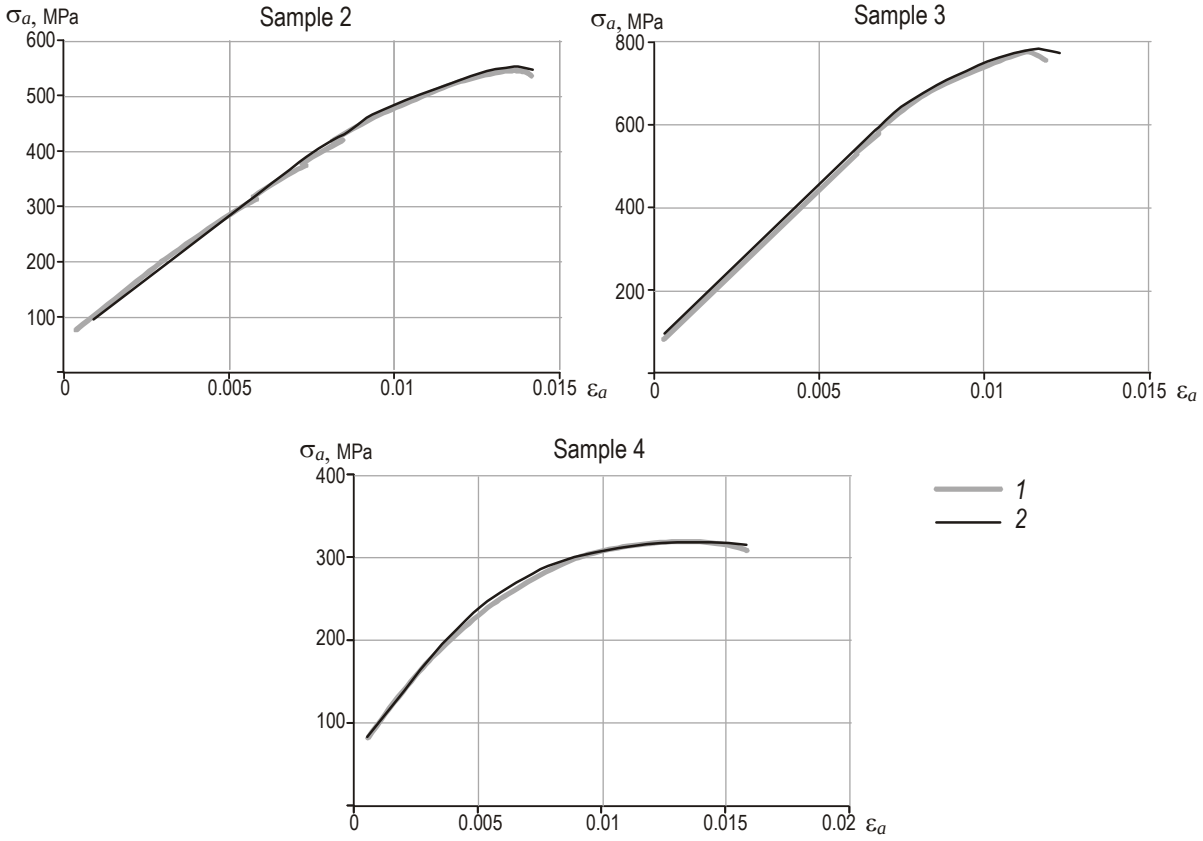

Fig. 6. Comparison of the experimental (curves *1*) and calculated (curves *2*) deformation diagrams with the variable internal friction angle for samples 2 (*top left*), 3 (*top right*), 4 (*bottom*)

Mohr-Coulomb diagram

When the elastic limit is reached, the rock fracturing starts. As it was shown by the previous analysis, the internal friction angle gradually increases from zero to the maximum value of φ=16.5° when the maximum axial load is reached, after which the softening starts and the localization of inelastic deformation is formed.

Condition (22) allows us to construct the Mohr-Coulomb diagram (Fig. 7).

Horizontal Mohr-Coulomb line corresponds to the initial friction angle φ=0°; inclined solid line is realized when the axial load reaches its maximum value at the angle of φ=16.5°, after which softening begins (see Fig. 4). Dashed lines between these lines correspond to the intermediate friction angles φ=5.5° and φ=11° (see Table 2).

The Mohr-Coulomb diagram obtained as a result of standard processing is shown as dashed line with the internal friction angle φ=27.3°. Thus, for a real sample, there are two limiting lines of Mohr-Coulomb criterion, unlike the idealized sample obtained on the basis of standard processing, for which there is only one Mohr-Coulomb line.

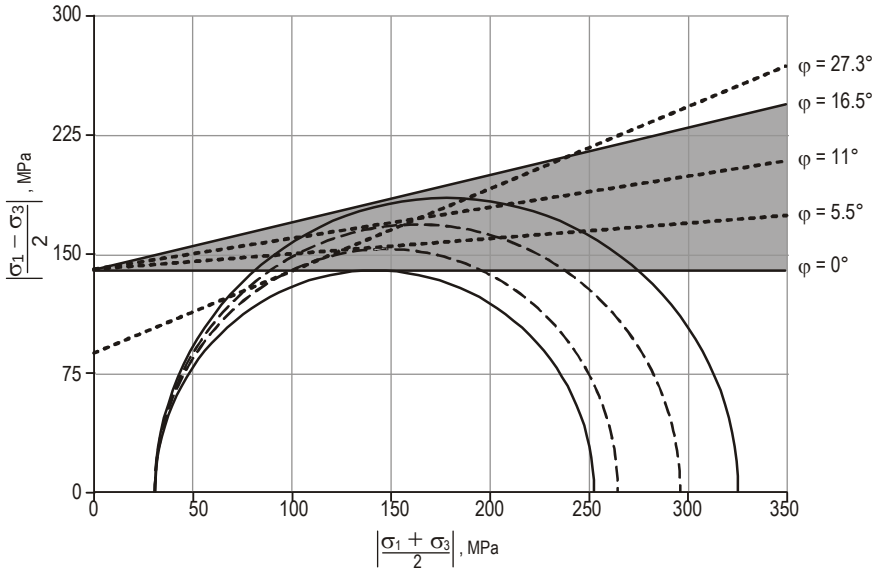

Fig. 7. Coulomb–Mohr diagrams corresponding to the different stages of deformation. Explanations in text

Within the plastic area marked with a gray color in Fig. 7, there is the formation of microcracks oriented at different angles. Angle ψ, formed by the normal to the crack plane with sample axis can be calculated by the formula

$$\psi = \frac{\pi/2 + \varphi}{2} \ . \tag{31}$$

Condition (31) characterizes the point position on the Mohr plane, determined as tangency point of Mohr circle built on the principal stresses σ_1 and σ_3, and line corresponding to the Mohr-Coulomb criterion (22). At zero angle of internal friction, the sliding sites are oriented at the angle of 45° to the sample axis; the change in the internal friction angle, accompanying the plastic deformation accumulation, leads to an increase of the angle between the normal to the sliding area and sample axis up to the value of ψ=53.2° (Fig. 8). Localization of plastic deformation occurs at the sites with orientation corresponding to the peak value of the internal friction angle.

Analysis of Fig. 7 and 8 allows to conclude that, as it was observed in the experiments [*Desrues, Viggiani*, 2004], cracks of different orientations were formed during the sample loading. Just one orientation of forming cracks corresponding to the angle of ψ=58.6° is allowed under conditions of standard method.

So, as long as loading increases the first cracks appear with the angle of orientation close to 45°; then cracks start to "slide" to the vertical axis. Let's estimate the percentage of microcracks of different orientations appearing under the plastic deformation increase. The total number of microcracks that formed in the sample during the time period between the start of plastic deformation accumulation moment t^{pl} and the moment of sample destruction t^{cr}, will be taken as 100 %.

Let the total accumulated plastic deformation Γ^{tot} in this interval be equal to $\Gamma^{pl}(t^{cr})$. Then the part of cracks with average orientation ψ_i, corresponding to the middle of the deformation interval $[t_i; t_{i+1}]$, where the internal friction angle changes from φ_i to φ_{i+1}, will be equal to $N^{cr}(\psi_i) = \left(\Gamma(t_{i+1}) - \Gamma(t_i)\right)/\Gamma^{tot}$.

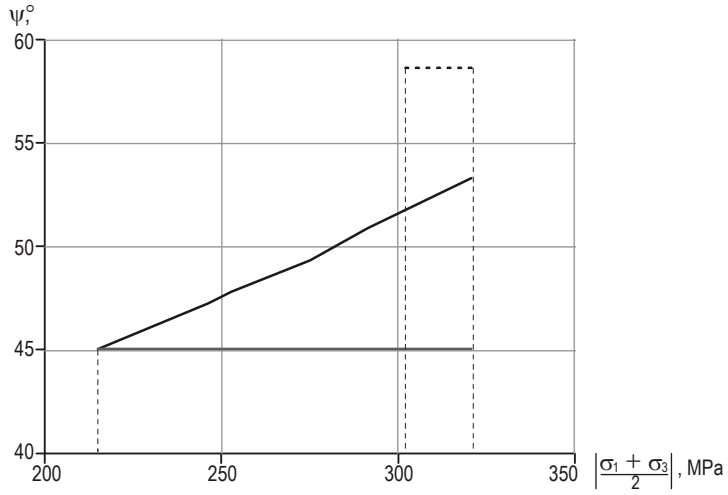

Fig. 8. Orientation of the fractures (ψ=58.6°) caused by plastic deformation in case of standard processing (dashed line). Solid lines are calculated using the approach suggested in this paper. These solid lines provide bounds for the area where fractures form with the normal vector oriented between ψ=45° and ψ=53.2° to the sample axis

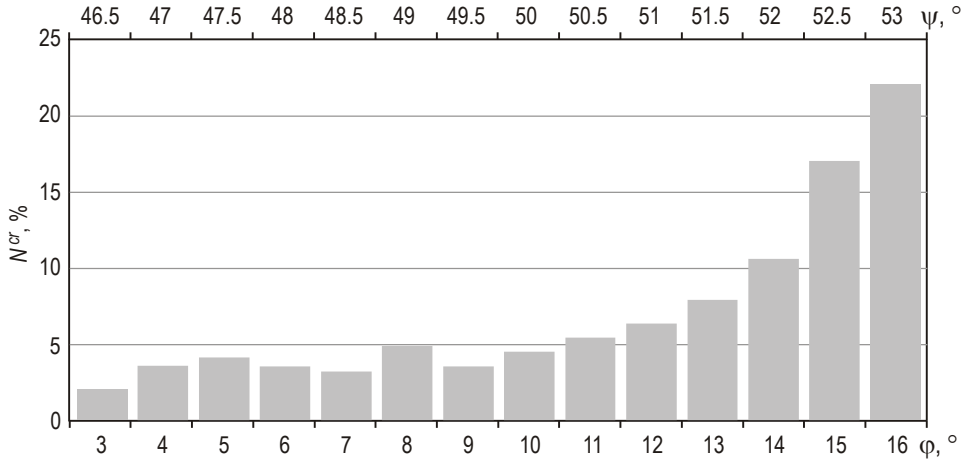

Fig. 9. Histogram of the micro-cracks orientations (in percent relative to the total number of microcracks that form in the sample). Top horizontal axis shows the mean angle between sample axis and normal to the crack plane ψ, calculated by (31)

Calculated estimation of fraction of fractures with certain orientation is shown in form of histogram in Fig. 9 (the minimum value of internal friction angle for the corresponding interval $\varphi_i = \varphi(t_i)$ is marked at the horizontal axis). The average values of angle between the sample axis and normal to the crack plane ψ, calculated by (31), are given in Fig. 9 on the additional horizontal axis above the histogram. It can be seen that the majority (up to 90%) of microcracks are formed under angles close to 53.2° which is related to the angle of the forming macrocrack.

Conclusions

One method for treating the results of triaxial tests of rock samples, that allows to take into account the inelastic deformation accumulation taking place in media with internal friction and dilatancy, due to usage of Prandtl-Reuss equations, was described.

Verification of the proposed method performed on a number of samples by comparing the results of triaxial tests with the results of numerical modelling, demonstrated the effectiveness of using the variable angle of internal friction for modelling deformations of rocks.

It is shown that the usage of variable friction angle in geomechanical models allows to take into account the localization of plastic deformation that cannot be done on the basis of traditional approach to processing experimental data.

It was established that there are two limiting lines of the Mohr-Coulomb criterion, restricting the plastic deformation area where the crack formation of different orientations takes place as it is observed in the experiments. Besides, the largest number of microcracks (up to 90 %) have angles close to ψ=53.2°, i.e. to the angle of forming macrocrack.

References

Desrues J. and Viggiani G. Strain localization in sand: an overview of the experimental results obtained in Grenoble using stereophotogrammetry *Int. J. Numer. Anal. Meth. Geomech*., 2004, vol. 28, pp. 279–321.

Fast Lagrangian Analysis of Continua in 3 Dimensions, Ver. 3.1, User's Manual. Itasca Consulting Group. Inc. FLAC3D. Minneapolis: Itasca, 2006.

Garagash I.A., and Nikolaevskii V.N. Non-associated flow laws and plastic deformation localization, *Advances in mechanics*, 1989, vol. 12, no. 1, pp. 131-183.

Garagash I.A., Conditions of the formation of regular systems of shear and compaction, *Russian Geology and Geophysics*, 2006, vol. 47, pp. 657-668.

Garagash I.A., Dubovskaya A.V., Bayuk I.O., Tikhotskiy S.A., Glubokovskikh S., Korneva D.A., and Berezina I.A. 3D geomechanical modeling of oil field on the basis of a model of the mechanical properties for the task of wells construction, *Proceedings of the SPE Russian Oil & Gas Exploration and Production*, Moscow, 2015. 11 p.

Garagash I.A., Nikolaevski V.N., and Dudley J.W. FLAC simulation of triaxial and compaction tests an unconsolidated reservoir sand. FLAC and Numerical Modeling in Geomechanics, *Proceedings of the International Symposium*, Balkema, 1999, pp. 505-510.

Kim M. M. and Ko H.Y. Multistage triaxial testing of Rocks, *Geotechnical Testing*, 1979, vol. 2, no. 2, pp. 98-105.

Nikolaevskii V.N. Governing equations of plastic deformation of a granular medium, *PMM*, 1971, vol. 35, no. 6, pp. 1070-1082.

Rice J.R., The Localization of Plastic Deformation, *Theoretical and Applied Mechanics*, Moscow: Mir Publishers, 1979, pp. 439-471.

Rudnicki J.W. and Rice J.R. Conditions for localization of deformation in pressure-sensitive dilatant materials, *J. Mech. Phys. Solids*, 1975, vol. 23, no. 6, pp. 371-390.

Tikhotsky S.A., Fokin I.V., Bayuk I.O., Beloborodov D.E., Berezina I.A., Dubinya N.V., Gafurova D.R., Krasnova M.A., Korost D.V., Makarova A.A., Patonin A.V., Ponomarev A.V., Khamidullin R.A., and Tselmovich V.A. Complex of laboratory core analysis at CPGR IPE RAS, *Nauka i tekhnologicheskiye razrabotki (Science and Technological Developments)*, 2017, vol. 96, no. 2, pp. 17-32.

Vermeer P.A. and de Borst R. Non-associated plasticity for soils, concrete and rock, *Heron*, 1984, vol. 29, no. 3, pp. 1-64.